Environmental impact assessment of Foz do Arelho sewage plume using MARES AUV

Patrícia Ramos
INESC Porto
Campus da FEUP, Rua Dr. Roberto Frias, 378
4200-465 Porto, Portugal
ISCAP - IPP
Rua Jaime Lopes Amorim, s/n
4465-004 S. Mamede de Infesta, Portugal
Email: pramos@inescporto.pt

Nuno Abreu
INESC Porto
Campus da FEUP, Rua Dr. Roberto Frias, 378
4200-465 Porto, Portugal
Email: nabreu@inescporto.pt

***Abstract*—Ocean sewage outfalls are major sources of contaminants to coastal ocean ecosystems. This method of disposal has advantages in terms of economy and relative societal impact, but it also raises important concerns about public health and ecosystem preservation. Autonomous Underwater Vehicles have already been shown to be very useful for monitoring routine of ocean outfalls. The major advantage of this technology over traditional methods is the ability to collect high-resolution data which can be very valuable for environmental impact assessment and comparison with plume prediction models. Once the data has been collected in the field it is necessary to extrapolate from monitoring samples to unsampled locations. Geostatistics has been successfully used to obtain information, for example, regarding the spatial distribution of soil properties. In this work geostatistics is used to model and map the spatial distribution of temperature and salinity measurements gathered by MARES AUV in a monitoring campaign to Foz do Arelho outfall, with the aim of distinguishing the effluent plume from the receiving waters and characterizing its spatial variability in the vicinity of the discharge. The results demonstrate that this methodology provides good estimates of the dispersion of effluent and it is therefore very valuable in assessing the environmental impact and managing sea outfalls.**

I. Introduction

Wastewaters are often discharged into coastal waters through outfall diffusers that efficiently dilute effluent and usually restrict any environmental impact within a small area. However, predicting this impact is difficult because of the complexity of the hydrodynamic processes that mix the wastewater and also because of the variability in oceanic conditions. Despite great improvements over the years in the understanding of these mixing processes, since models are now available that can make reasonable predictions under steady-state conditions [1], many aspects remain unknown and unpredictable. For this reason, much effort has been recently devoted to improve ways of monitoring and characterizing sewage plumes under a variety of oceanographic conditions. Autonomous Underwater Vehicles have already been shown to be very useful for performing high-resolution surveys of small features such as outfall plumes. Some of the advantages of these platforms include: easier field logistics, low cost per deployment, good spatial coverage, sampling over repeated sections and the ability to perform feature-based or adaptive sampling. Once the data has been collected in the field it is necessary to extrapolate from monitoring samples to unsampled locations. Geostatistics has been successfully used to obtain information, for example, regarding the spatial distribution of soil properties. Besides giving estimated values at unsampled locations, it provides a measure of the accuracy of the estimate, which is a significant advantage over traditional methods used to assess pollution. In this work geostatistics is used to model and map the spatial distribution of temperature and salinity measurements gathered by MARES AUV in a monitoring campaign to Foz do Arelho outfall, with the aim of distinguishing the effluent plume from the receiving waters, characterizing its spatial variability in the vicinity of the discharge and estimating dilution. In the next section MARES AUV's physical and operating characteristics are fully described. In the third section, after giving a brief explanation about ordinary kriging method, we present the results obtained in the geostatistical study. Finally we discuss the results and give the conclusions.

II. MARES AUV

MARES (Modular Autonomous Robot for Environment Sampling) AUV has been successfully used to monitor sea outfalls discharges ([2][3]) (see Fig. 1). MARES is 1.5 m long, has a diameter of 8-inch and weighs about 40 kg in air. It features a plastic hull with a dry mid body (for electronics and batteries) and additional rings to accommodate sensors and actuators. Its modular structure simplifies the system's development (the case of adding sensors, for example). It is propelled by two horizontal thrusters located at the rear and two vertical thrusters, one at the front and the other at the rear. This configuration allows for small operational speeds and high maneuverability, including pure vertical motions. It is equipped with an omnidirectional acoustic transducer and an electronic system that allows for long baseline navigation. The vehicle can be programmed to follow predefined trajectories while collecting relevant data using the onboard sensors. A Sea-Bird Electronics 49 FastCAT CTD had already been

978-1-61284-4577-0088-0/11/$26.00 ©2011 IEEE

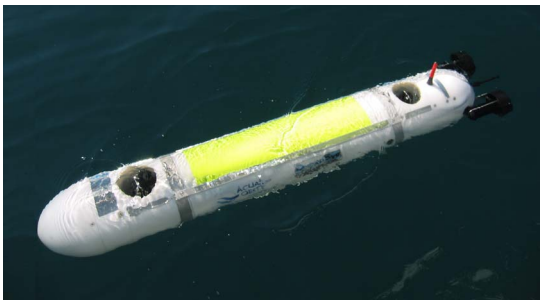

Fig. 1. AUV MARES.

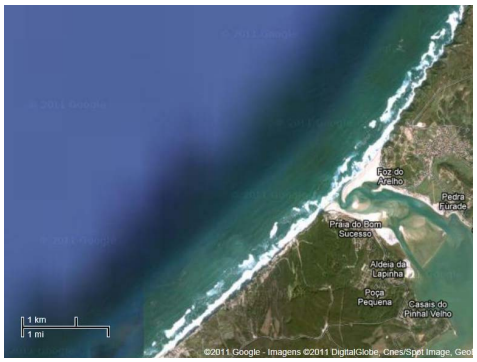

Fig. 2. Map of the study area.

installed onboard the MARES AUV to measure conductivity, temperature and depth. MARES' missions for environmental monitoring of wastewater discharges are conducted using GUI software that fully automates the operational procedures of the campaign [4]. By providing visual and audio information, this software guides the user through a series of steps which include: (1) real time data acquisition from CTD and ADCP sensors, (2) effluent plume parameter modeling using the CTD and ADCP data collected, (3) automatic path creation using the plume model parameters, (4) acoustic buoys and vehicle deployment, (5) automatic acoustic network setup and (6) real time tracking of the AUV mission.

III. Material and Methods

A. Study area

The study site is shown in Fig. 2. The Foz do Arelho outfall is located off the Portuguese west coast near the Óbidos lagoon. In operation since June 2005, is presently discharging about 0.11 m^3/s of mainly domestic wastewater from the WWTPs of Óbidos, Carregal, Caldas da Rainha, Gaeiras, Charneca and Foz do Arelho, but it can discharge up to 0.354 m^3/s. The total length of the outfall, including the diffuser, is 2150 m. The outfall pipe, made of HDPE, has a diameter of 710 mm. The diffuser, which consists of 10 ports spaced 8 or 12 meters apart, is 93.5 m long. The ports, nominally 0.175 m in diameter, are discharging upwards at an angle of 90º to the pipe horizontal axis; the port height is about 1 m. The outfall direction is southeast-northwest (315.5º true bearing) and is discharging at a depth of about 31 m. In that area the coastline itself runs at about a 225º angle with respect to true north and the isobaths are oriented parallel to the coastline. A seawater quality monitoring program for the outfall has already started in May 2006. Its main purposes are to evaluate the background seawater quality both in offshore and nearshore locations around the vicinity of the sea outfall and to follow the impacts of wastewater discharge in the area. During the campaign the discharge remained fairly constant with an average flowrate of approximately 0.11 m^3/s. The operation area specification was based on the outputs of a plume prediction model [1] which include mixing zone length, spreading width, maximum rise height and thickness. The model inputs are, besides the diffuser physical characteristics, the water column stratification, the current velocity and direction, and the discharge flowrate. Information on density stratification was obtained from a vertical profile of temperature and salinity acquired in the vicinity of the diffuser two weeks before the campaign. The water column was weakly stratified due to both low-temperature and salinity variations. The total difference in density over the water column was about 0.13 σ-unit. The current direction of 110º was estimated based on predictions of wind speed and direction of the day of the campaign. A current velocity of 0.12 m/s was estimated based on historic data. The effluent flowrate consider for the plume behavior simulation was 0.11 m^3/s. According to the predictions of the model, the plume was spreading 1 m from the surface, detached from the bottom and forming a two-layer flow. The end of the mixing zone length was predicted to be 141 m downstream from the diffuser. Fig. 3 shows a plan view of the AUV operation area, mainly in the northeast direction from the diffuser, covering about 20000 m^2. The AUV collected CTD data at 1.5 m and 3 m depth, in accordance to the plume minimum dilution hight prediction. During the mission the vehicle transited at a fairly constant velocity of 1 m/s (2 knots) and recorded data at a rate of 16 Hz. Maximum vertical oscillations of the AUV in performing the horizontal trajectories were less than 0.5 m (up and down).

B. Geostatistical analysis

1) Ordinary kriging: The ordinary kriging method is often referred to using the acronym BLUE which stands for *Best Linear Unbiased Estimator*. It is *Linear* because its estimates are weighted linear combinations of the available data. It is *Unbiased* since it expects to obtain a mean error equal to 0 and it is *Best* because it aims to minimize the variance of the errors. In order to estimate the unknown value at any point, the model is a random stationary function that consists of $n+1$ random variables (with the same probability law), one for the value at each of the n sample locations, $Z(\mathbf{x}_1), Z(\mathbf{x}_2), \ldots, Z(\mathbf{x}_n)$, and one for the unknown value at the point that is being estimated ([5][6]). The estimate of $Z(\mathbf{x}_0)$ is defined as a weighted linear combination of the random variables at the n sampled locations:

$$\hat{Z}(\mathbf{x}_0) = \sum_{i=1}^{n} w_i \cdot Z(\mathbf{x}_i). \quad (1)$$

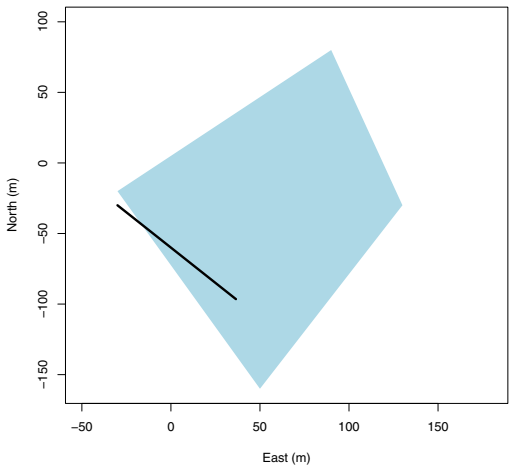

Fig. 3. AUV operation area.

Assuming that all random variables have the same expected value, m, the expected value of the estimation error is:

$$E\left[\varepsilon(\mathbf{x}_0)\right] = E[Z(\mathbf{x}_0) - \hat{Z}(\mathbf{x}_0)] = m\left(1 - \sum_{i=1}^{n} w_i\right). \quad (2)$$

Setting this expected value to 0, to ensure an unbiased estimate, results in:

$$\sum_{i=1}^{n} w_i = 1. \quad (3)$$

Assuming that all random variables have the same variance, σ^2, the variance of the estimation error is:

$$var\left[\varepsilon(\mathbf{x}_0)\right] = \sigma^2 - 2\sum_{i=1}^{n} w_i C_{i0} + \sum_{i=1}^{n}\sum_{j=1}^{n} w_i w_j C_{ij} \quad (4)$$

where $C_{i0} = cov\left[Z(\mathbf{x}_i), Z(\mathbf{x}_0)\right]$ and $C_{ij} = cov\left[Z(\mathbf{x}_i), Z(\mathbf{x}_j)\right]$, $i, j = 1, 2, \ldots, n$. The minimization of the error variance, constrained by the unbiasedness condition Eq. 3, is solved using the Lagrange multipliers method which produces the following system of equations:

$$\underbrace{\begin{bmatrix} C_{11} & \ldots & C_{1n} & 1 \\ \vdots & \vdots & \ddots & \vdots \\ C_{n1} & \ldots & C_{nn} & 1 \\ 1 & \ldots & 1 & 0 \end{bmatrix}}_{(n+1)\times(n+1)} \cdot \underbrace{\begin{bmatrix} w_1 \\ \vdots \\ w_n \\ \mu \end{bmatrix}}_{(n+1)\times 1} = \underbrace{\begin{bmatrix} C_{10} \\ \vdots \\ C_{n0} \\ 1 \end{bmatrix}}_{(n+1)\times 1} \quad (5)$$

$$\mathbf{C} \cdot \mathbf{w} = \mathbf{D}$$

The set of weights $w_1, \ldots, w_n$ and the Lagrange multiplier μ, that will produce an unbiased estimate of $Z(\mathbf{x}_0)$ with the minimum error variance are then given by:

$$\mathbf{w} = \mathbf{C}^{-1} \cdot \mathbf{D}. \quad (6)$$

Therefore, the minimized error variance, usually called the ordinary kriging variance, is given by:

$$var\left[\varepsilon(\mathbf{x}_0)\right] = \sigma^2 - \mathbf{w}^T \cdot \mathbf{D}. \quad (7)$$

2) Block kriging: A consideration in many environmental applications has been that ordinary kriging usually exhibits large prediction errors ([7]). This is due to the larger variability in the observations. When predicting averages over larger areas, i.e. within blocks, much of the variability averages out and consequently block mean values have lower prediction errors. If the blocks are not too large the spatial patterns do not disappear. The block kriging system is similar to the point kriging system given by Eq. 5 ([5]). The matrix $\mathbf{C}$ is the same since it is independent of the location at which the block estimate is required. The covariances for the vector $\mathbf{D}$ are point-to-block covariances. Supposing that the mean value over a block V is approximated by the arithmetic average of the N point variables contained within that block ([5][8]), i.e.

$$Z_V \approx \frac{1}{N}\sum_{j=1}^{N} Z(\mathbf{x}_j), \quad (8)$$

the point-to-block covariances required for vector $\mathbf{D}$ are

$$\bar{C}_{iV} = cov\left[Z(\mathbf{x}_i), Z_V\right] = \frac{1}{N}\sum_{j=1}^{N} C_{ij}, \qquad \forall i = 1, 2, \ldots, n. \quad (9)$$

The block kriging variance is

$$\sigma_V^2 = \bar{C}_{VV} - \left(\sum_{i=1}^{n} w_i \bar{C}_{iV} + \mu\right), \quad (10)$$

where $\bar{C}_{VV}$ is the average covariance between pairs of points within V :

$$\bar{C}_{VV} = \frac{1}{N^2}\sum_{i=1}^{N}\sum_{j=1}^{N} C_{ij}. \quad (11)$$

An equivalent procedure, that can be computationally more expensive than block kriging, is to obtain the block estimate by averaging the N kriged point estimates within the block ([5][8]).

3) Spatial continuity: Assuming that the random function is stationary, all pairs of random variables, separated by a distance and direction $\mathbf{h}$ (known as lag), have the same joint probability distribution. Therefore, the covariance function is ([5][6]):

$$C(\mathbf{h}) = E\left[Z(\mathbf{x})Z(\mathbf{x}+\mathbf{h})\right] - \left\{E\left[Z(\mathbf{x})\right]\right\}^2. \quad (12)$$

Geostatisticians usually define the spatial continuity of the sample data set using the semivariogram, or simply a variogram, which is defined as:

$$\gamma(\mathbf{h}) = \frac{1}{2}E\left[\left\{Z(\mathbf{x}) - Z(\mathbf{x}+\mathbf{h})\right\}^2\right] = \frac{1}{2}var\left[Z(\mathbf{x}) - Z(\mathbf{x}+\mathbf{h})\right], \quad (13)$$

and solve the system of equations (5) using the following relation:

$$\gamma(\mathbf{h}) = C(\mathbf{0}) - C(\mathbf{h}) = \sigma^2 - C(\mathbf{h}). \quad (14)$$

The widely used estimator of the variogram, known as Matheron's method-of-moments estimator (MME), is ([9]):

$$\gamma(\mathbf{h}) = \frac{1}{2N(\mathbf{h})} \sum_{i=1}^{N(\mathbf{h})} [Z(\mathbf{x}_i) - Z(\mathbf{x}_i + \mathbf{h})]^2 . \quad (15)$$

where $Z(\mathbf{x}_i)$ is the value of the variable of interest at location x_i and $N(\mathbf{h})$ is the number of pairs of points separated by the particular lag $\mathbf{h}$. Cressie and Hawkins [10] developed an estimator of the variogram that should be robust to the presence of outliers and enhance the variogram's spatial continuity. It also has the advantage of not spreading the effect of outliers when computing the maps. This estimator (CRE) is defined as follows [10]:

$$\gamma(\mathbf{h}) = \frac{1}{2} \times \frac{\left\{ \frac{1}{N(\mathbf{h})} \sum_{i=1}^{N(\mathbf{h})} |Z(\mathbf{x}_i) - Z(\mathbf{x}_i + \mathbf{h})|^{1/2} \right\}^4}{0.457 + \frac{0.494}{N(\mathbf{h})} + \frac{0.045}{[N(\mathbf{h})]^2}}. \quad (16)$$

Once the variogram has been calculated, a function must be fit to it. The most commonly used variogram models are the spherical model, the exponential model, the Gaussian model and the Matern model ([5]).

4) Cross-validation: Cross-validation is a procedure that is used to compare the performance of several competing models. It starts by splitting the data set into two sets: a modeling set and a validation set. The modeling set is then used for variogram modeling and kriging on the locations of the validation set. Finally the observations of the validation set are compared to their predictions using the following standard measures ([5]):

$$\mathrm{ME} = \frac{1}{m} \sum_{i=1}^{m} [z(x_i) - \hat{z}(x_i)] , \quad (17)$$

$$\mathrm{MSE} = \frac{1}{m} \sum_{i=1}^{m} [z(x_i) - \hat{z}(x_i)]^2 , \quad (18)$$

$$\mathrm{RMSE} = \sqrt{\frac{1}{m} \sum_{i=1}^{m} [z(x_i) - \hat{z}(x_i)]^2}, \quad (19)$$

The Mean Error (ME) should be close to zero and the Mean Squared Error (MSE) and the Root Mean Squared Error (RMSE) should be as small as possible. A scatterplot of true versus predicted values provides additional evidence on how well an estimation method has performed. Typically the set of points should come as close as possible to the line $y = x$, a 45-degree line passing through the origin on the scatterplot. The coefficient of determination R^2 is a good index for summarizing how close the points on the scatterplot come to falling on the 45-degree line passing through the origin ([5]). R^2 should be close to one.

TABLE I
SUMMARY STATISTICS OF TEMPERATURE MEASUREMENTS.

	Temperature@1.5 m	Temperature@3.0 m
Samples	20,026	10,506
Mean	15.463°C	15.469°C
Median	15.466°C	15.472°C
Minimum	15.359°C	15.393°C
Maximum	15.562°C	15.536°C
Coefficient of skewness	-0.31	-0.70
Coefficient of variation	0.002	0.001

IV. SPATIAL ANALYSIS

The geostatistical analysis was carried out using an application that was developed based on the *R* statistical software ([11]) and on the Gstat package of *R* ([7]). This application guides the user through several steps that perform the geostatistical analysis. More details about this software application may be found in [12]. In order to obtain elementary knowledge about the temperature and salinity data sets, conventional statistical analysis was conducted (see the results in Table I and Table II). At the depth of 1.5 m the temperature ranged from 15.359°C to 15.562°C and at the depth of 3 m the temperature ranged from 15.393°C to 15.536°C. The mean value of the data sets was 15.463°C and 15.469°C, respectively at the depths of 1.5 m and 3 m, which was very close to the median value that was respectively 15.466°C and 15.472°C. The coefficient of skewness is relatively low (-0.309) for the 1.5 m data set and not very high (-0.696) for the 3 m data set, indicating that in the first case the histogram is approximately symmetric and in the second case that distribution is only slightly asymmetric. The very low values of the coefficient of variation (0.002 and 0.001) reflect the fact that the histograms do not have a tail of high values. At the depth of 1.5 m the salinity ranged from 35.957 psu to 36.003 psu and at the depth of 3 m the salinity ranged from 35.973 psu to 36.008 psu. The mean value of the data sets was 35.991 psu and 35.996 psu, respectively at the depths of 1.5 m and 3 m, which was very close to the median value that was respectively 35.990 and 35.998 psu. The coefficient of skewness is not to much high in both data sets (-0.63 and -1.1) indicating that distributions are only slightly asymmetric. The very low values of the coefficient of variation (0.0002 and 0.0001) reflect the fact that the histograms do not have a tail of high values. The ordinary kriging method works better if the distribution of the data values is close to a normal distribution. Therefore, it is interesting to see how close the distribution of the data values comes to being normal. Fig. 4 shows the plots of the normal distribution adjusted to the histograms of the temperature measured at depths of 1.5 m and 3 m, and Fig. 5 shows the plots of the normal distribution adjusted to the histograms of the salinity measured at depths of 1.5 m and 3 m. Apart from some erratic high values it can be seen that the histograms are reasonably close to the normal distribution.

For the purpose of this analysis, the temperature and the

TABLE II
SUMMARY STATISTICS OF SALINITY MEASUREMENTS.

	Salinity@1.5 m	Salinity@3.0 m
Samples	20,026	10,506
Mean	35.991 psu	35.996 psu
Median	35.990 psu	35.998 psu
Minimum	35.957 psu	35.973 psu
Maximum	36.003 psu	36.008 psu
Coefficient of skewness	-0.63	-1.1
Coefficient of variation	0.0002	0.0001

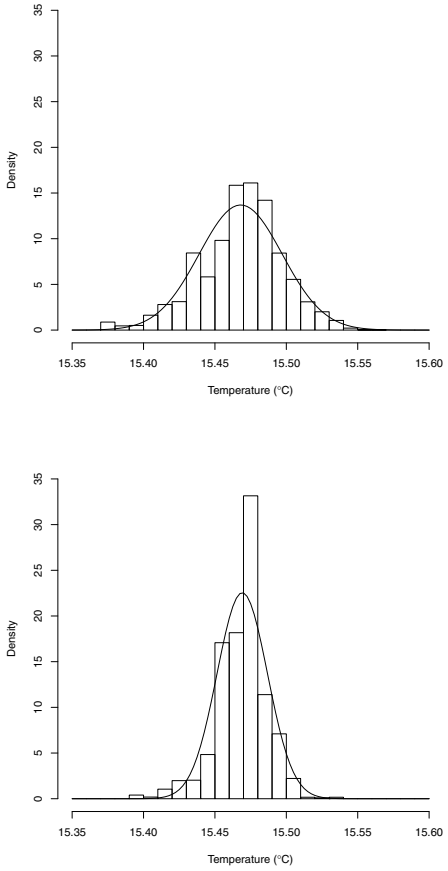

Fig. 4. Histograms of temperature measurements at depths of 1.5 m (top) and 3 m (bottom).

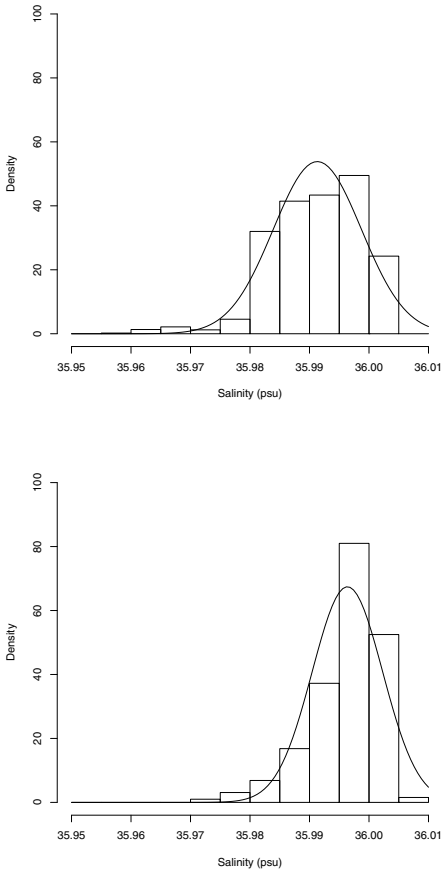

Fig. 5. Histograms of salinity measurements at depths of 1.5 m (top) and 3 m (bottom).

salinity measurements were divided into a modeling set (comprising 90% of the samples) and a validation set (comprising 10% of the samples). Modeling and validation sets were then compared, using Student's-t test, to check that they provided unbiased sub-sets of the original data. Furthermore, sample variograms for the modeling sets were constructed using the MME estimator and the CRE estimator. This robust estimator was chosen to deal with outliers and enhance the variogram's spatial continuity. An estimation of semivariance was carried out using a lag distance of 2 m. Table III and Table IV show the parameters of the fitted models to the omnidirectional sample variograms constructed using MME and CRE estimators. All the variograms were fitted to Matern models (for several shape parameters ν) with the exception to the salinity data measured at the depth of 3 m. The range value (in meters) is an indicator of extension where autocorrelation exists. The variograms of salinity show significant differences in range. The autocorrelation distances are always larger for the CRE estimator which may demonstrate the enhancement of the variogram's spatial continuity. All variograms have low nugget values which indicates that local variations could be captured due to the high sampling rate and to the fact that the variables under study have strong spatial dependence. Anisotropy was investigated by calculating directional variograms. However, no anisotropy effect could be shown.

The block kriging method was preferred since it produced smaller prediction errors and smoother maps than the point kriging. Using the 90% modeling sets of the two depths, a two-dimensional ordinary block kriging, with blocks of 10×10 m^2, was applied to estimate temperature at the locations of the 10% validation sets. The validation results for both parameters measured at depths of 1.5 m and 3 m depths are shown in

TABLE III
PARAMETERS OF THE FITTED VARIOGRAM MODELS FOR TEMPERATURE MEASURED AT DEPTHS OF 1.5 AND 3.0 M.

Depth	Variogram Estimator	Model	Nugget	Sill	Range
1.5	MME	Matern ($\nu = 0.4$)	0.000	0.001	75.0
	CRE	Matern ($\nu = 0.5$)	0.000	0.002	80.1
3.0	MME	Matern ($\nu = 0.3$)	0.000	0.0002	101.3
	CRE	Matern ($\nu = 0.7$)	0.000	0.002	107.5

TABLE IV
PARAMETERS OF THE FITTED VARIOGRAM MODELS FOR SALINITY MEASURED AT DEPTHS OF 1.5 AND 3 M.

Depth	Variogram Estimator	Model	Nugget	Sill	Range
1.5	MME	Matern ($\nu = 0.6$)	0.436	11.945	134.6
	CRE	Matern ($\nu = 0.6$)	0.153	10786.109	51677.1
3.0	MME	Matern ($\nu = 0.8$)	0.338	11.724	181.6
	CRE	Gaussian	0.096	120.578	390.1

Table V and Table VI. At both depths temperature was best estimated by the variogram constructed using CRE. Salinity at the depth of 1.5 m was best estimated by the variogram constructed using CRE and at the depth of 3 m was best estimated using the Gaussian model with the MME. The difference in performance between the two estimators: block kriging using the MME estimator (MBK) or block kriging using the CRE estimator (CBK) is not substantial. Fig. 6 shows the omnidirectional sample variograms for temperature at the depth of 1.5 m and 3 m fitted by the preferred models. Fig. 7 shows the omnidirectional sample variograms for salinity at the depth of 1.5 m and 3 m fitted by the preferred models.

Fig. 8 and Fig. 9 show the scatterplots of true versus estimated values for the most satisfactory models. The dark line is the 45° line passing through the origin and the discontinuous line is the OLS (Ordinary Least Squares) regression line. These plots show that observed and predicted values are highly positively correlated. The R^2 value for the temperature at the depth of 1.5 m was 0.9211 and the RMSE was 0.0088248°C, and at the depth of 3 m was 0.8827 and the RMSE was 0.0058316°C (Table V). The R^2 value for the salinity at the depth of 1.5 m was 0.9513 and the RMSE was 0.0016435 psu, and at the depth of 3 m was 0.8982 and the RMSE was 0.0019793 psu (Table VI).

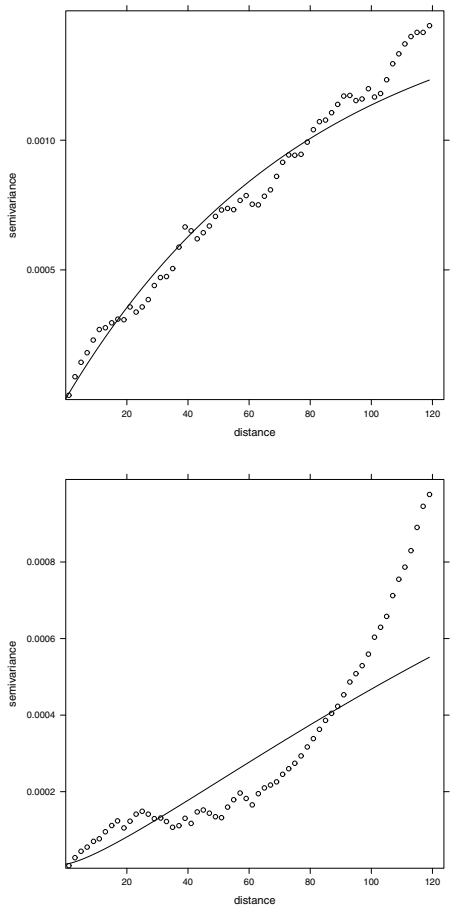

Fig. 6. Variograms for temperature at depths of 1.5 m (top) and 3 m (bottom).

TABLE V
CROSS-VALIDATION RESULTS FOR THE TEMPERATURE MAPS AT DEPTHS OF 1.5 AND 3 M.

Depth	Method	R^2	ME	MSE	RMSE
1.5	MBK	0.9184	2.0174e-4	8.0530e-5	8.9739e-3
	CBK[a]	0.9211	1.6758e-4	7.7880e-5	8.8248e-3
3.0	MBK	0.8748	1.0338e-4	3.6295e-5	6.0244e-3
	CBK[a]	0.8827	0.6538e-4	3.4008e-5	5.8316e-3

[a] The preferred model.

TABLE VI
CROSS-VALIDATION RESULTS FOR THE SALINITY MAPS AT DEPTHS OF 1.5 AND 3 M.

Depth	Method	R^2	ME	MSE	RMSE
1.5	MBK	0.9471	3.1113e-5	2.8721e-6	1.6947e-3
	CBK[a]	0.9513	-3.1579e-5	2.7010e-6	1.6435e-3
3.0	MBK[a]	0.8982	-7.1735e-5	3.9175e-6	1.9793e-3
	CBK	0.7853	-8.1264e-5	8.2589e-6	2.8738e-3

[a] The preferred model.

Fig. 10 and Fig. 11 show the block kriged maps of temperature on a 2×2 m^2 grid using the preferred models. Fig. 12 and Fig. 13 show the block kriged maps of salinity on a 2×2 m^2 grid using the preferred models. In the 1.5 m kriged map the temperature ranges between 15.407°C and 15.523°C and the average value is 15.469°C, which is in accordance with the measurements (range 15.359°C–15.562°C and average 15.463°C). In the 3 m kriged map the temperature ranges between 15.429°C and 15.502°C and the average value is 15.467°C, which is in accordance with the measurements (range 15.393°C–15.536°C and average 15.469°C). In the 1.5 m kriged map the salinity ranges between 35.960 psu and 36.004 psu and the average value is 35.992 psu, which

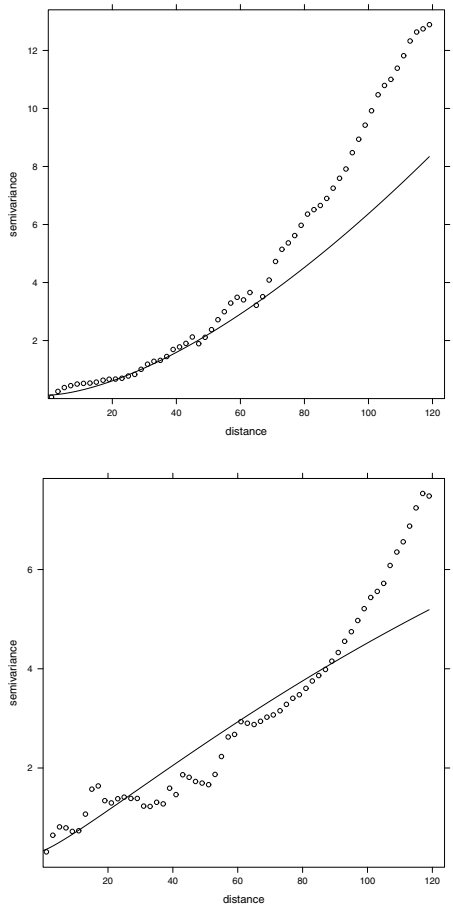

Fig. 7. Variograms for salinity at depths of 1.5 m (top) and 3 m (bottom).

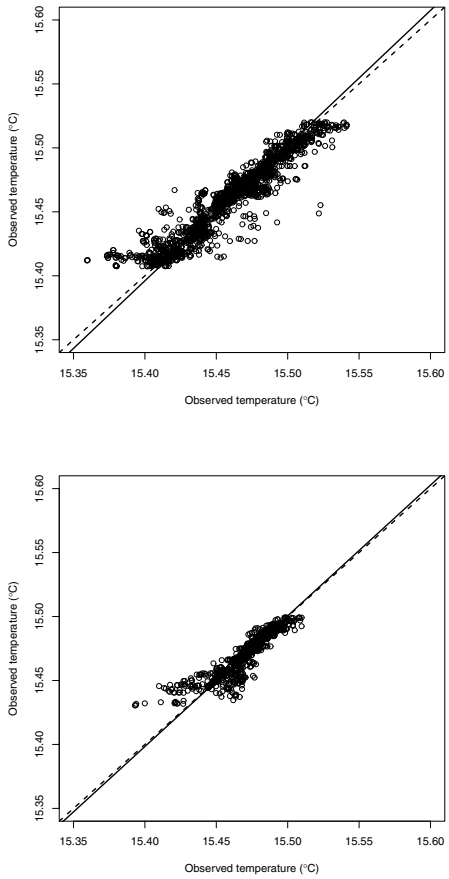

Fig. 8. Predicted versus observed temperature at the depths of 1.5 m (top) and 3 m (bottom) using the preferred models.

is in accordance with the measurements (range 35.957psu–36.003psu and average 35.991 psu). In the 3 m kriged map the salinity ranges between 35.977 psu and 36.004 psu and the average value is 35.995 psu, which is in accordance with the measurements (range 35.973psu–36.008psu and average 35.996 psu). As predicted by the plume prediction model, the effluent was found dispersing close to the surface. From the temperature and salinity kriged maps it is possible to distinguish the effluent plume from the background waters. It appears as a region of lower temperature and lower salinity when compared to the surrounding ocean waters at the same depth. At the depth of 1.5 m the major difference in temperature compared to the surrounding waters is about -0.116^{o}C while at the depth of 3 m this difference is about -0.073^{o}C. At the depth of 1.5 m the major difference in salinity compared to the surrounding waters is about -0.044 psu while at the depth of 3 m this difference is about -0.027 psu. It is important to note that these very small differences in temperature and salinity were detected due to the high resolution of the CTD sensor. [13] observed temperature and salinity anomalies in the plume in the order, respectively of -0.3^{o}C and -0.1 psu, when compared with the surrounding waters within the same depth range. The small plume-related anomalies observed in the maps are evidence of the rapid mixing process. Due to the large differences in density between the rising effluent plume and ambient ocean waters, entrainment and mixing processes are vigorous and the properties within the plume change rapidly [1]. The effluent plume was found northeast from the diffuser beginning, spreading downstream in the direction of current. Using the navigation data, we could later estimate current velocity and direction and the values found were, respectively, 0.4 m/s and 70^{o}C, which is in accordance with the location of the plume.

V. Conclusion

Through geostatistical analysis of temperature and salinity obtained by an AUV at depths of 1.5 m and 3 m in an ocean outfall monitoring campaign it was possible to produce kriged maps of the sewage dispersion in the field. The spatial variability of the sampled data has been analyzed and the results indicated an approximated normal distribution of the temperature and salinity measurements, which is desirable. The Matheron's classical estimator and Cressie and Hawkins' robust estimator were then used to compute the omnidirec-

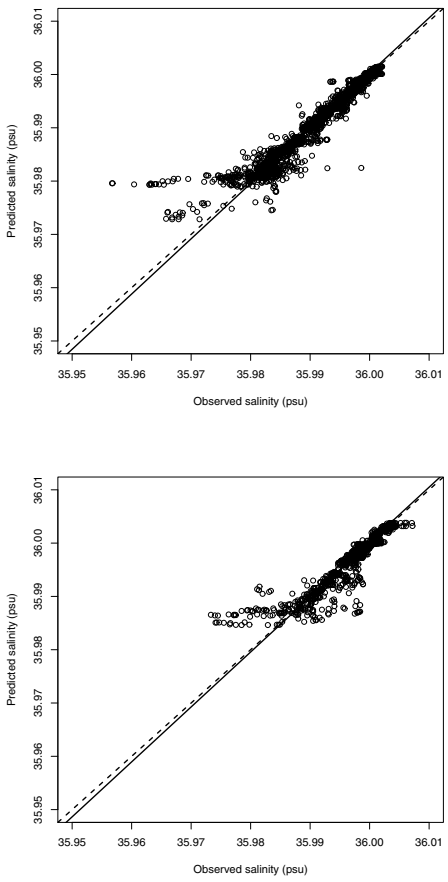

Fig. 9. Predicted versus observed salinity at the depths of 1.5 m (top) and 3 m (bottom) using the preferred models.

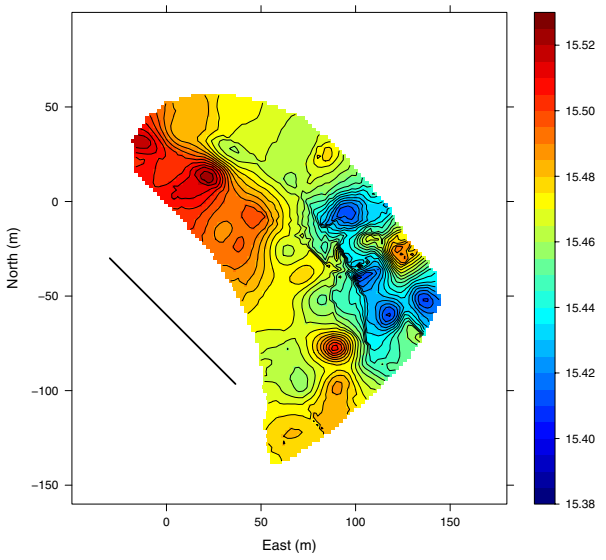

Fig. 10. Prediction map of temperature distribution at the depth of 1.5 m.

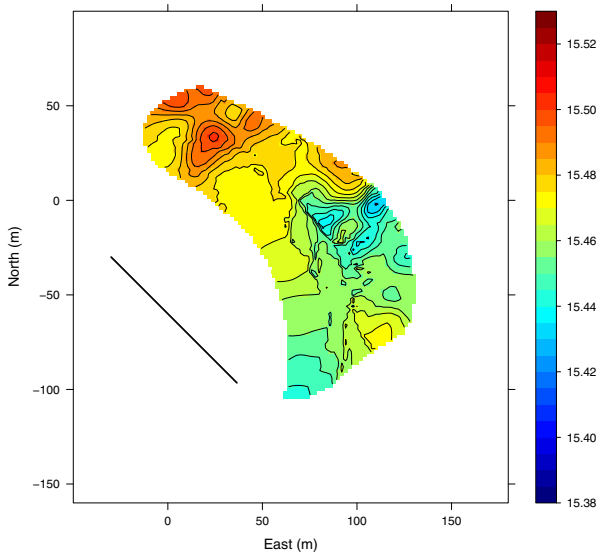

Fig. 11. Prediction map of temperature distribution at the depth of 3 m.

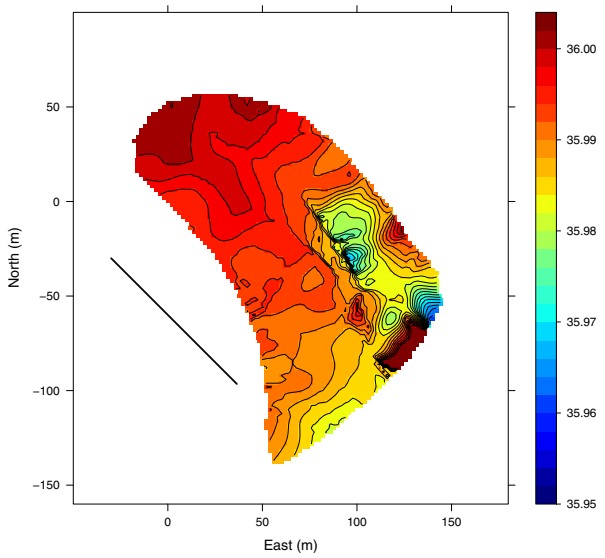

Fig. 12. Prediction map of salinity distribution at the depth of 1.5 m.

tional variograms that were fitted to Matern models (for several shape parameters) and to a Gaussian model. The performance of each competing model was compared using a split-sample approach. In the case of temperature, the validation results, using a two-dimensional ordinary block kriging, suggested the Matern model ($\nu = 0.5$–1.5 m and $\nu = 0.7$–3 m) with semivariance estimated by CRE. In the case of salinity, the validation results, using a two-dimensional ordinary block kriging, suggested the Matern model ($\nu = 0.6$–1.5 m and $\nu = 0.8$–3 m) with semivariance estimated by CRE, for the depth of 1.5 m, and with semivariance estimated by MME,

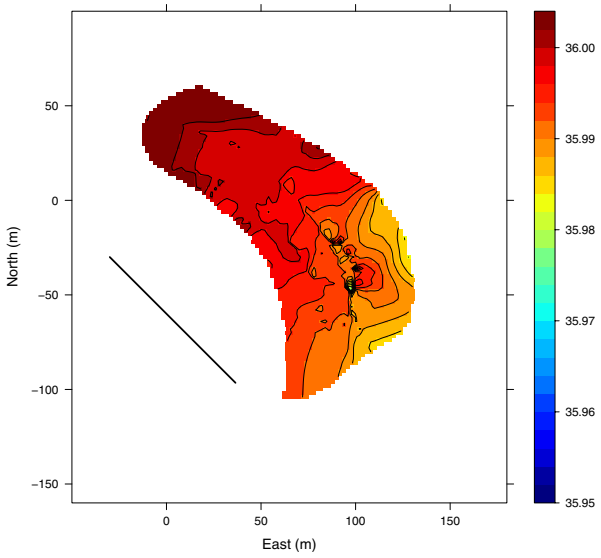

Fig. 13. Prediction map of salinity distribution at the depth of 3 m.

for the depth of 3 m. The difference in performance between the two estimators was not substantial. Block kriged maps of temperature and salinity at depths of 1.5 m and 3 m show the spatial variation of these parameters in the area studied and from them it is possible to identify the effluent plume that appears as a region of lower temperature and lower salinity when compared to the surrounding waters. These results demonstrate that geostatistical methodology can provide good estimates of the dispersion of effluent that are very valuable in assessing the environmental impact and managing sea outfalls.

ACKNOWLEDGMENT

This work was partially funded by the Foundation for Science and Technology (FCT) under the Program for Research Projects in all scientific areas (Programa de Projectos de Investigação em todos os domínos científicos) in the context of WWECO project - Environmental Assessment and Modeling of Wastewater Discharges using Autonomous Underwater Vehicles Bio-optical Observations (Ref. PTDC/MAR/74059/2006).

REFERENCES

[1] C. D. Hunt, A. D. Mansfield, M. J. Mickelson, C. S. Albro, W. R. Geyer, and P. J. W. Roberts, "Plume tracking and dilution of effluent from the Boston sewage outfall," *Marine Environmental Research*, vol. 70, pp. 150–161, 2010.

[2] P. Ramos and N. Abreu, "Using an AUV for Assessing Wastewater Discharges Impact: An Approach Based on Geostatistics," *Marine Technology Society Journal*, vol. 45, no. 2, 2011.

[3] P. Ramos, M. V. Neves, and F. L. Pereira, "Mapping and Initial Dilution Estimation of a Sewage Outfall Plume using an Autonomous Underwater Vehicle," *Continental Shelf Research*, no. 27, pp. 583–593, 2007.

[4] N. Abreu, A. Matos, P. Ramos, and N. Cruz, "Automatic interface for AUV mission planning and supervision," in *MTS/IEEE International Conference Oceans 2010*, Seattle, USA, September 20-23 2010.

[5] E. H. Isaaks and R. M. Srivastava, *Applied geostatistics*, O. U. Press, Ed., New York Oxford, 1989, ISBN 0-19-505012-6-ISBN 0-19-505013-4 (pbk.).

[6] N. Cressie, *Statistics for spatial data*, A. W. I. Publication, Ed., New York, 1993.

[7] R. S. Bivand, E. J. Pebesma, and V. Gómez-Rubio, *Applied spatial data analysis with R*, S. S. U. R, Ed., 2008, ISBN: 97 -0-387-78170-9.

[8] P. Goovaerts, *Geostatistics for natural resources evaluation, Applied Geostatistics Series*, O. U. Press, Ed., 1997, ISBN13: 9780195115383, ISBN10: 0195115384.

[9] G. Matheron, *Les variables régionalisées et leur estimation: une application de la théorie des fonctions aléatoires aux sciences de la nature*, F. Masson, Ed., Paris, 1965.

[10] N. Cressie and D. M. Hawkins, "Robust estimation of the variogram, I," *Jour. Int. Assoc. Math. Geol.*, vol. 12, no. 2, pp. 115–125, 1980.

[11] R Development Core Team, "The R Project for Statistical Computing," 2011. [Online]. Available: http://www.r-project.org/

[12] N. Abreu and P. Ramos, "An integrated application for geostatistical analysis of sea outfall discharges based on R software," in *MTS/IEEE International Conference Oceans 2010*, Seattle, USA, September 20-23 2010.

[13] L. Washburn, B. H. Jones, A. Bratkovich, T. D. Dickey, and M.-S. Chen, "Mixing, Dispersion, and Resuspension in Vicinity of Ocean Wastewater Plume," *Journal of Hydraulic Engineering, ASCE*, vol. 118, no. 1, pp. 38–58, Jan. 1992.